SCIENTIFIC REPORTS
nature research

OPEN

Rutile $Ru_xTi_{1-x}O_2$ nanobelts to enhance visible light photocatalytic activity

S. Mihai[1], D. L. Cursaru[1*], D. Matei[1], A. M. Manta[1], R. Somoghi[2] & G. Branoiu[1]

We herein report on the synthesis by a facile sol-gel method without templates for preparing rutile $Ru_xTi_{1-x}O_2$ (x = 0.16; 0.07; 0.01) nanobelts with exposed (001) facets. The rutile nanobelts with exposure (001) facets, favor the separation photogenerated electron-hole pairs and inhibit the recombination of the electron-hole pairs resulting in the increase of the number of main superoxide and hydroxyl radicals. The photocatalytic properties of the rutile $Ru_xTi_{1-x}O_2$ nanobelts were evaluated by discoloring of MB (methylene blue) dye under sunlight irradiation at an intensity of 40000 lx. It was also done a thorough interface analysis to determine the band energy.

Titanium dioxide (TiO_2) has been extensively investigated due to its chemical stability, low cost, catalytic properties, photocatalytic properties, environmental clean-up by organic compound mineralization[1] and because it is a renewable energy generator used for efficient hydrogen production[2–4].

TiO_2 has four crystalline polymorphs, anatase, rutile, brookite and TiO_2 (B) (biphasic based on anatase). Anatase and anatase biphasic TiO_2 have been extensively investigated in photocatalysis[5] under various forms and morphologies: microspheres, nanoflows, nanotrees and nanobelts[6–8].

One of the objectives of photocatalysis is the efficient use and conversion of solar light, this is done by doping classical photocatalysts with noble metals (Au, Ag, Pt, etc.)[7,9,10] or other oxides (RuO_2)[11,12]. Also, understanding the principles of crystal growth is a major challenge for many researchers, surface science is an intensely studied field. In the last decade, the science of anatastic surface has attracted attention due to the special properties of the surface, the differences in reactivity and surface energy[13]. Yang to al.[13] were the promoters of the TiO_2 anatase crystal synthesis with a high percentage (47% by weight) of facets (001), using hydrogen fluoride. Nanobelts structures are considered 1D nanostructures. The dimensional study plays an important role in determining material properties and is a huge challenge for researchers. 1D nanostructures have been extensively investigated due to their distinctive properties related to 0D and 2D materials. 1D nanostructures show two important properties: fast electronic transport and effective load transfer[14]. Synthesis of 1D nanoparticles depends on several factors: chemical method, *p*H and temperature, while the catalytic activity depends mainly on the properties of the surface[8]. The increased interest in the controlled synthesis of the exposed face exposed TiO_2 particles (001) is due to a high photocatalytic activity compared to (101) faces[15]. The study research of Zhao *et al.* have shown that surface energy of rutile TiO_2 facets is $\gamma(001) > \gamma(100) > \gamma(101)$ (0,90 J m-2 > 0,53 J m-2 > 0,44 J m-2)[14]. The chemical dissociation of the water molecules is energetically favored on the plane (001), and the hydroxyl radicals on the TiO_2 surface react much more easily with the dissociated molecules of the organic compounds[14].

In this paper, it was developed a facile sol-gel method without templates for preparing rutile.

$Ru_xTi_{1-x}O_2$ nanobelts crystals with controlled morphologies. The nanobelts have a layer structure which is beneficial for the introduction of heteroatoms, as an example Ru, because RuO_2 adopts the rutile structure. Introduction of the metal ions into the crystalline structure of TiO_2 nanobelts, expands the absorption edge to the visible light range to enhance, therefore we propose the introduction of ruthenium into the crystal for the extend of the absorption to the visible light range.

Results

The crystalline phases structures of rutile TiO_2 and rutile $Ru_xTi_{1-x}O_2$ nanobelts are shown in Fig. 1. RuO_2 shows a rutile structure and it has lattice parameters similar to those of TiO_2 rutile, therefore no new peaks were observed in the diffraction spectrums of nanobelts structures, regardless of Ru doping concentration.

[1]Petroleum – Gas University of Ploiesti, 39 Bucharest Av., 100680, Ploiesti, Romania. [2]National Research and Development Institute for Chemistry and Petrochemistry, 202 Splaiul Independentei, 060021, Bucharest, Romania. *email: dianapetre@upg-ploiesti.ro

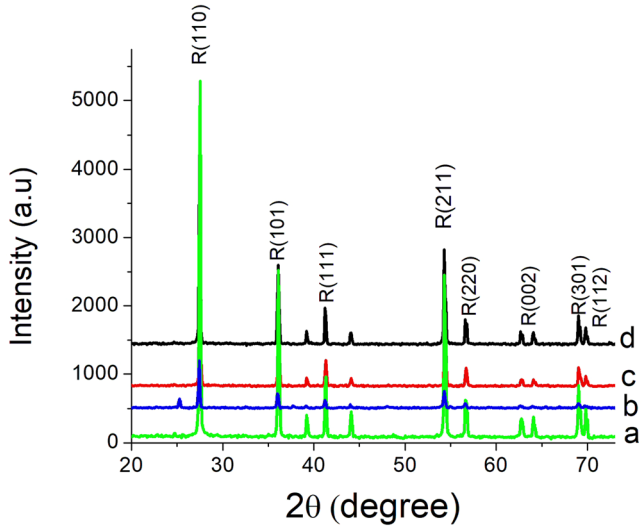

Figure 1. XRD patterns of $Ru_xTi_{1-x}O_2$ nanobelts a(x = 0); b(x = 0.01); c(x = 0.07); d(x = 0.16).

Sample	Space group	Z	Lattice parameters (Å)		d_{110} (Å)	Cell Volume (Å^3)	Crystal Density (g/cm^3)
			a (=b)	c			
$Ti_{1-x}Ru_xO_2$, x = 0.01	P42/mnm	2	4.587	2.957	3.243	62.240	4.314
$Ti_{1-x}Ru_xO_2$, x = 0.07	P42/mnm	2	4.592	2.959	3.247	62.466	4.463
$Ti_{1-x}Ru_xO_2$, x = 0.16	P42/mnm	2	4.595	2.967	3.250	62.474	4.648

Table 1. The crystalline phase composition and lattice parameters from Rietveld refinement.

Whatever of the Ru doping concentration, the typical diffraction peaks which appear at 2θ = 28°, 36°, 42°, 55°, 57°, 63°, 64°, 68°, 69°could be assigned as the (110); (101); (111); (211); (220); (002); (310); (301); (112) diffraction lines corresponding to the rutile phase. The crystalline phase composition and lattice parameters from rutile nanobelts, having a tetragonal phase with lattice parameters a = b from 4.587 to 4.595 Å, and c = 2.957 to 2.967 Å is obtained with very high crystalline quality. The crystalline phase composition and lattice parameters from Rietveld refinement are summarized in Table 1.

It should be noted that the larger lattice constants and d-spacing values are due to upon Ru doping. This is due to the larger ionic radius of Ru than that of Ti in the rutile, the structural relaxation follows the Vegard's law[16]. The d-spacing value of the rutile sample for (110) plane is in agreement to the interatomic dimension observed at HRTEM microscopy. Figure 2 shows the HRTEM images of $Ru_xTi_{1-x}O_2$ (x = 0.16) nanobelts sample. The TEM images confirm the formation of one-dimensional nanobelts nanostructures. Rutile TiO_2 nanobelts have very small thicknesses, widths of 6–20 nm and can be 100–200 nm in length.

The HRTEM image shows the (101) and (002) atomic planes with lattice spacings of 3.499 Å (1/r) and 4.255 Å (1/r), respectively[17]. The interfacial angle between these two crystalline facets was found to be 67.27° and it was determined by Fast-Fourier Transform (FFT) image (Fig. 2). Deviation with one degree may be due to ruthenium from the crystalline lattice. These results even if less than the theoretical value, reveal that the interfacial angle between rutile is in good agreement with the theoretical value of the angle between the (101) and (001) planes. HRTEM images suggest that the prepared sample behaved like a well-crystallized heterostructure nanobelts.

Rutile $Ru_xTi_{1-x}O_2$ nanobelts have an octahedral arrangement, where either Ti or Ru atoms prefer a coordination number of 6. The layered arrangements of octahedrons facilitate their growth in the (001) direction as nanobelt like geometry[14].

The UV-Vis diffuse reflectance spectroscopy (DRS) spectra of all samples are shown in Fig. 3A. The DRS method is employed to determine the band gap energy for photocatalysts. The intense absorption feature in the range of 200 nm–408 nm is characteristic of the TiO_2 and corresponds to the band gap energy of 3.2 eV as for rutile phase. The visible absorption band in the range 408–627 nm corresponds to the band gap energy from 2 to 3.2 eV and can be assigned to charge transfer transition of the donor ($Ru^{4+} \rightarrow Ru^{5+} + e^-$, $Ru^{3+} \rightarrow Ru^{4+} + e^-$) or acceptor ($Ru^{4+} \rightarrow Ru^{3+} + h^+$) type[18,19].

This suggests that rutile $Ru_xTi_{1-x}O_2$ photocatalysts could be active in the visible light region. The specters UV-vis from rutile $Ru_xTi_{1-x}O_2$ photocatalysts were transformed to the absorption specters according to the Kubelka Munk theory: $[\boldsymbol{F}(\boldsymbol{R}_\infty) \cdot \boldsymbol{h\nu}]^{1/2}$ (Fig. 4). The optical band gap energies of the photocatalysts can be approximated from the plot of $[\boldsymbol{F}(\boldsymbol{R}_\infty) \cdot \boldsymbol{h\nu}]^{1/2}$ versus hν (photon energy) and were estimated from the intercept of the tangent with the abscissa axis yielding the band gap energies. It can be observed that the gap energies band is presented in Fig. 4 compared to the bulk rutile TiO_2 of 3.2 eV. The bandgap energies decreased from 3.2 eV for rutile TiO_2 to 2.55 eV, 2.68 eV 3.07 eV for $Ru_xTi_{1-x}O_2$ x = 0.16, x = 0.07 and x = 0,01 respectively.

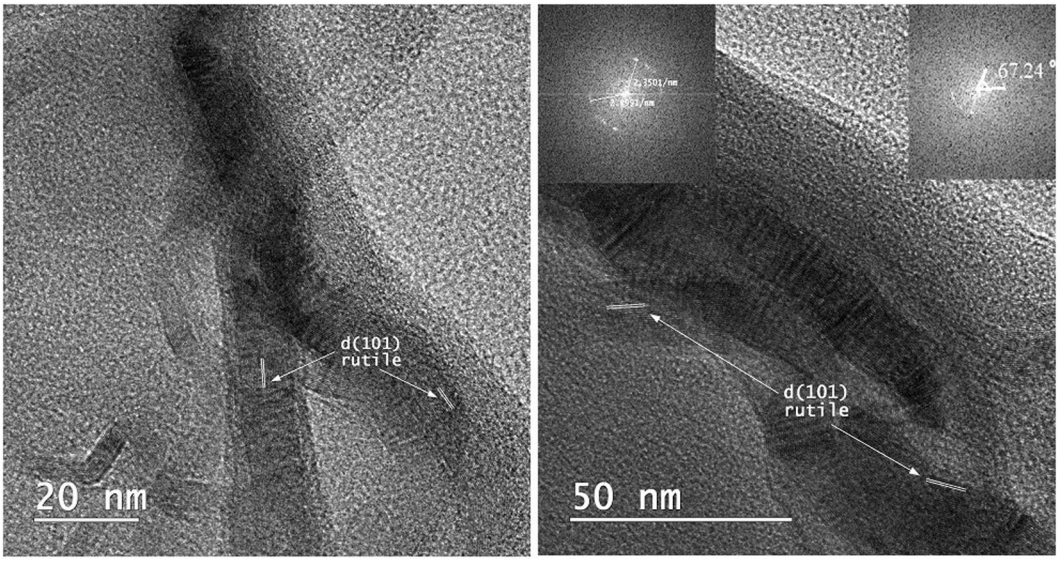

Figure 2. HRTEM images for $Ru_xTi_{1-x}O_2$ (x = 0.16) nanobelts.

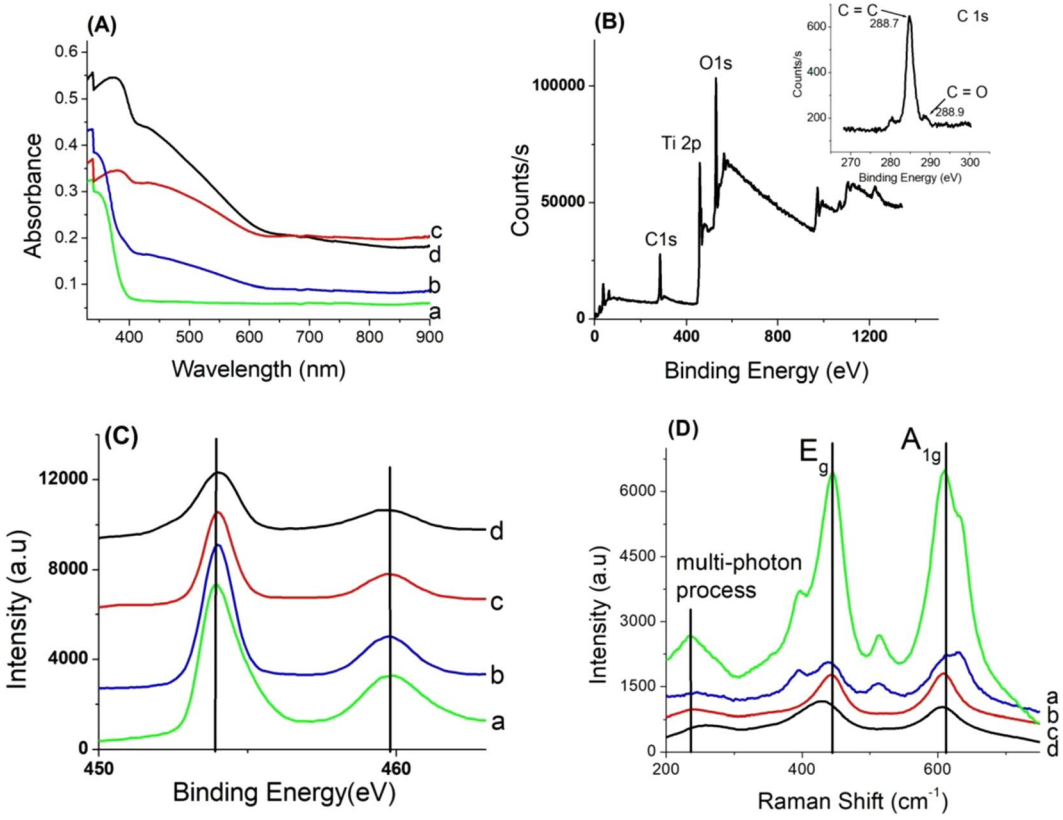

Figure 3. (**A**) UV-vis spectra of $Ru_xTi_{1-x}O_2$ nanobelts; (**B**) XPS survey spectrum of $Ru_xTi_{1-x}O_2$ (x = 0.16) nanobelts; (**C**) High resolution core XPS spectra of $Ru_xTi_{1-x}O_2$ nanobelts a(x = 0); b(x = 0.01); c(x = 0.07); d(x = 0.16); (**D**) Raman spectrum of $Ru_xTi_{1-x}O_2$ nanobelts.

XPS measurements have been performed to analyze the surface composition and oxidation states of Ti and Ru in the samples. The survey spectrum for the $Ru_xTi_{1-x}O_2$ (x = 0.16), with the highest ruthenium content (Fig. 3B), confirms the complete removal of chlorine in the samples TiO_2 doped. The absence of the peaks in area 197.9 eV and 199.5 eV (Cl 2p3/2 and Cl 2p1/2) were observed. Figure 3C shows the XPS spectra of Ti 2p on the surface of each sample. The binding energies at 454.0 and 459.7 eV (Ti 2p3/2 and Ti 2p1/2) correspond to octahedral coordinated Ti^{4+} state[19,20]. The energy difference between the two peaks is 5,7 eV which is consistent with the energy

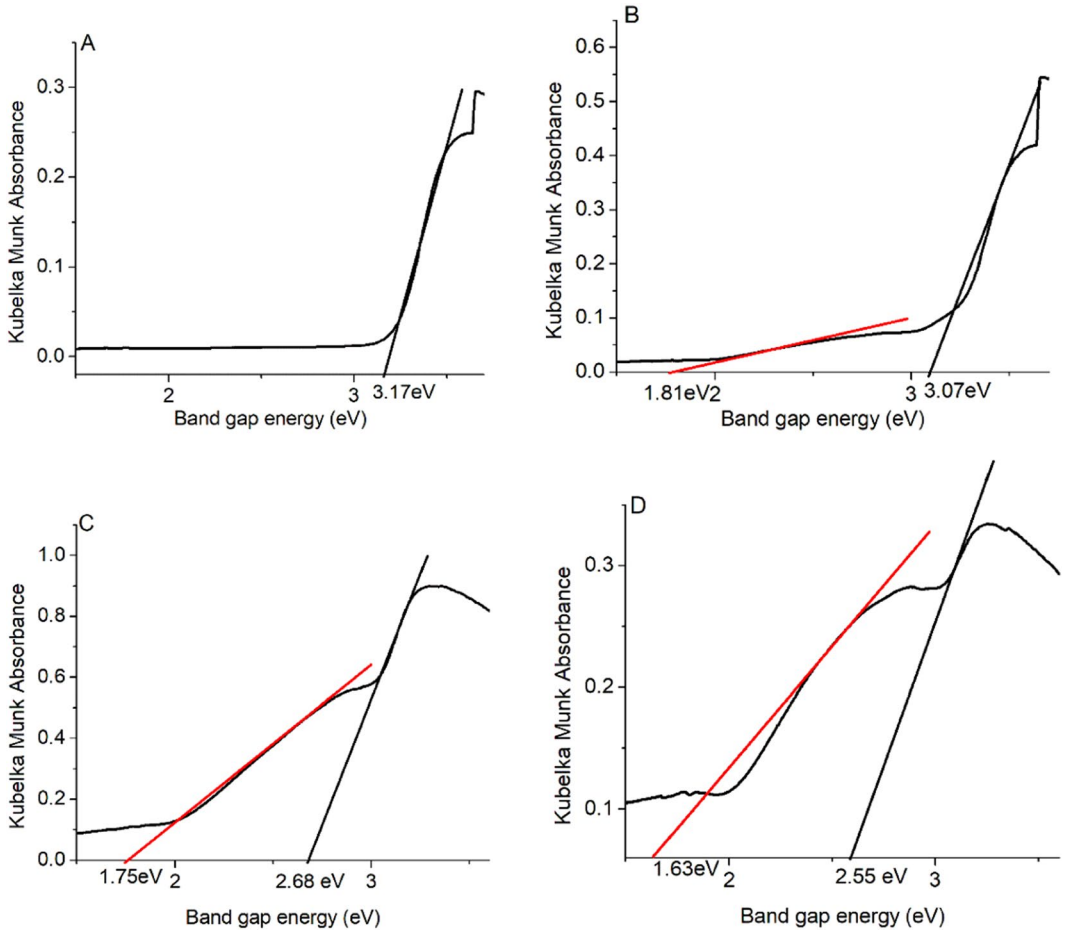

Figure 4. Determination of energy band gap of $Ru_xTi_{1-x}O_2$ nanobelts a (x = 0); b (x = 0.01); c (x = 0.07); d (x = 0.16).

difference between the level of spin-orbit splitting coupling effect. e (Fig. 3C). The substitution of Ru ions into the TiO_2 lattice can induce electronic structure.

The Raman spectra for rutile $Ru_xTi_{1-x}O_2$ photocatalysts are displayed in Fig. 3D, where two bands features of tetragonal rutile TiO_2 (space group D_{4h}) at 445 and 610 cm^{-1} were assigned to E_g (planar O-O vibration) and A_{1g} (Ti-O stretch) modes 20. The broad band at 235 cm^{-1} was attributed to the multiple photon scattering process. The absence of the peaks to features attributable to RuO_2 from 528 cm^{-1} and 646 cm^{-1} corresponds to E_g and A_{1g} modes[21], was evident in all of the samples, confirming the lattice substitution of the RuO_2 in the rutile TiO_2. Ruthenium doping induces a low red-shifts with increasing Ru concentration in all of the samples, probably due to the formation of oxygen defects or Ru-O-Ti linkages (Fig. 3D).

The photocatalytic properties of the rutile $Ru_xTi_{1-x}O_2$ nanobelts have been evaluated by photocatalytic degradation of methylene blue (MB) under sunlight at the 40000 lx intensity. The photocatalytic results are displayed in Fig. 5A. It was observed that the photodegradation process of methylene blue took place faster in the presence of rutile doped with ruthenium compared with undoped rutile. The increase of ruthenium content gave a decrease of the band gap that can be correlated with the increase absorption to the visible light range, and respectively enhance of the photocatalytic activity. It was observed that the photodegradation process of methylene blue took place faster in the presence of rutile $Ru_xTi_{1-x}O_2$ (x = 0.16) nanobelts compared to the other synthesized photocatalysts. It can be observed that after irradiation for 90 min, about 90% of the methylene blue has been degraded for the $Ru_{0.16}Ti_{0.84}O_2$ nanobelts which are above the results of the rutile TiO_2 (74 wt.%).

The kinetic curves of sunlight MB degradation over each catalyst are depicted in Fig. 5B and show that the degradation of MB dye follows pseudo first-order kinetics law, $\ln C/C_0 = k_{app}t$, where k_{app} is the pseudo-first order constant rate.

The constant rate k_{app}, was determined by plotting the $\ln C/C_0$ versus irradiation time. It can be observed that with increasing of the ruthenium content the constant rate k_{app} rises from 0.0125 min^{-1} to 0.0227 min^{-1} (Table 2).

On the basis of the experimental results, a possible mechanism of the enhanced photocatalytic activity over the rutile $Ru_xTi_{1-x}O_2$ is proposed in Fig. 6.

The enhanced photocatalytic activity caused by ruthenium doping and to the ability of Ru to capture the photogenerated holes on the TiO_2 (valence band). The conduction band can be calculated by using the empirical equation[22]:

Ecb = Evb − Eg and Evb of semiconductor were estimated by the following equation:

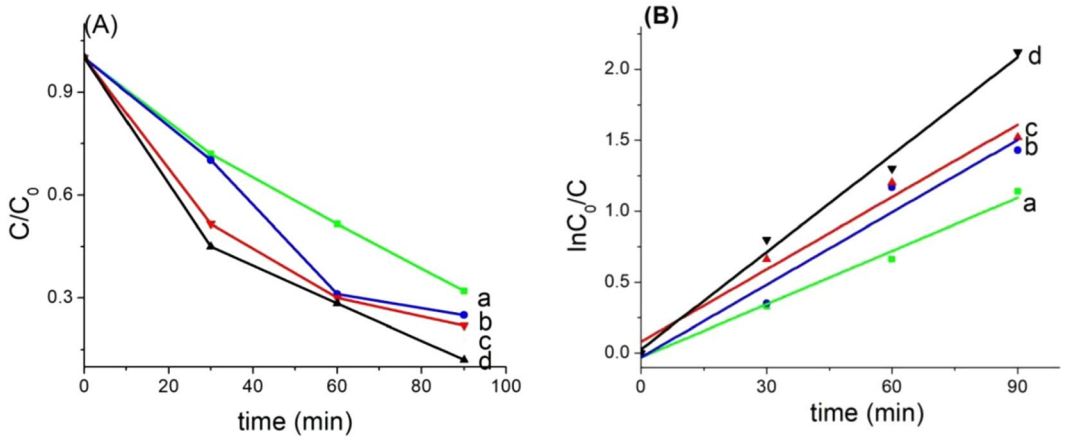

Figure 5. (**A**) The C/C_0 versus time curves of photocatalytic degradation of MB; (**B**) Photocatalytic performances of $Ru_xTi_{1-x}O_2$ nanobelts a(x = 0); b(x = 0.01); c(x = 0.07); d(x = 0.16).

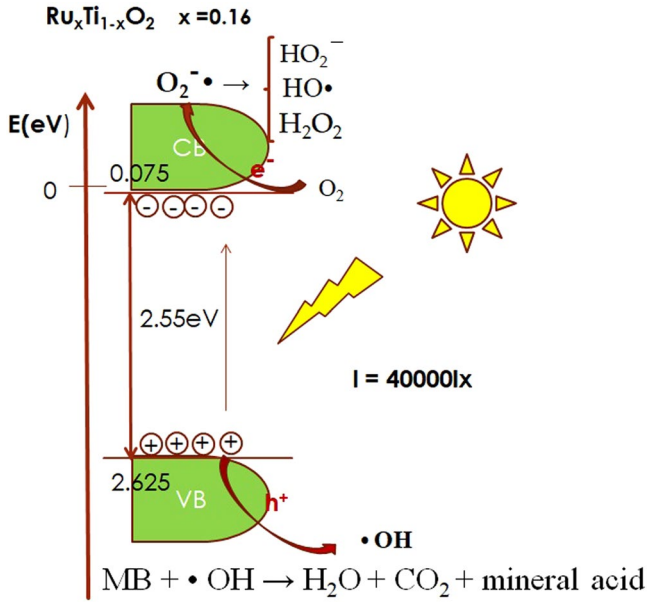

Figure 6. Mechanism of $Ru_xTi_{1-x}O_2$ nanobelts photocatalysis.

k_{app}	$Ru_xTi_{1-x}O_2$ (x = 0.16)	$Ru_xTi_{1-x}O_2$ (x = 0.07)	$Ru_xTi_{1-x}O_2$ (x = 0.01)	TiO_2
k_{app} MB (min^{-1})	0.02273	0.0170	0.0168	0.0125

Table 2. The rate constant k_{app} of $Ru_xTi_{1-x}O_2$ nanobelts.

Evb = X − Ee + 1/2Eg, where Ecb is the conduction band, Evb is the valence band, X the geometric mean of the Mulliken, Ee is the energy of free electrons on the hydrogen scale (~4.5 eV) and Eg is the bandgap value of semiconductor, respectively. The values of Ecb, Evb are displayed in Table 3.

It can be observed that hydrogen peroxide and peroxide radicals can form. The photocatalytic process is shown in Fig. 6. Excitaded electrons under sunlight jumped from VB (valence band) to CB (conduction band) and generate charge carriers (electron-hole pairs). Due to the nanobelts structure, the electron-hole pairs are moved to the photocatalyst surface, where electrons and holes are involved in redox reactions on the surface. The photocatalytic degradation efficiency can be due to the reactive (001) facets, these having a strong ability to dissociate water molecules to form hydrogen peroxide and peroxide radicals, contributors in the photo-oxidation process[16].

Energy (eV)	$Ru_xTi_{1-x}O_2$ (x = 0.16)	$Ru_xTi_{1-x}O_2$ (x = 0.07)	$Ru_xTi_{1-x}O_2$ (x = 0.01)	TiO_2
E_g	2.55	2.68	3.07	3.17
X	5.85	5.83	5.81	5.80
E_{CB}	0.075	−0.01	−0.225	−0.285
E_{VB}	2.625	2.67	2.845	2.885

Table 3. The values Ecb, Evb of $Ru_xTi_{1-x}O_2$ nanobelts.

Discussions

$Ru_xTi_{1-x}O_2$ nanobelts were synthesized by the sol-gel method by doping TiO_2 with RuO_2. The reaction was carried out in HCl medium (c > 10 mol/l), which facilitated the formation of nanobelts nanostructures. RuO_2 has been chosen for doping since both RuO_2 and TiO_2 have the same crystalline crystal structure, the crystalline parameters have almost equal values, coordinate number 6 for both Ti and Ru. From the diffraction spectrum, the rutile phase is observed for all nanobelts with high crystallinity. Also, doping TiO_2 with ruthenium has a double role: decrease the bandgap and facilitating light from the visible field in the photocatalysis process, as well as to inhibit the recombination of the electron-hole pairs.

UV-vis absorption spectra were transformed using the Kubelka Munk function and the values of the bandgap energy for all samples with which the values of conduction bands and valence bands were calculated. In both the UV-vis and the transformed Kubelka Munk spectra, there are two types of transitions: interband between the 2p orbitals of the oxygen and the orbitals of the ruthenium and an interband type d-d between the orbitals of Ru (1.65–1.81 eV)[23–25]. TiO_2 is considered a n-type semiconductor. There is a decrease in the bandgap from 3.17 to 2.55 eV as the content of Ru concentration increases in the samples, there is also an increase in the conductive band value, respectively, a decrease of valence value of nanobelts as the increase in doping with Ru. This favors the splitting of water and the formation of oxidoreduction species. Corroborated with the shape of nanostructures with surface exposure (001) facets showed the performance of efficient photocatalysts in the degradation of organic compounds. Doping with Ru induces a stress in the crystal of $Ru_xTi_{1-x}O_2$, which is revealed by an angle deviation of 68.3° to 67.3° for the (001) facets. Crystal stress is also noticeable in Raman spectra by easily moving to redshifts the bands assigned to Eg and A1g corresponding to the rutile phase of TiO_2. The XPS spectrum shows a slight (low) displacement of the corresponding Ti $2p_{3/2}$ and Ti $2p_{1/2}$ blue-shifts spectra due to ruthenium doping. The high performance of the photocatalysts is due both to the nanobelts form and to the ruthenium doping and the visible light access to the photodegradation process. The superoxide and hydroxyl radicals obtained on the photocatalyst surface favor the mineralization reaction of the organic dye by in CO_2 and H_2O.

In conclusion, the rutile $Ru_xTi_{1-x}O_2$ nanobelts with exposure of (001) facets were successfully synthesized by a simple sol-gel method chemical route using hydrochloric acid and ethanol as capping and stabilizing agents. The superior photocatalytic activity of rutile nanobelts can be assigned to the band gap energy reduction from 3.2 to 2.55 eV and due to its small size, high surface area and of exposed highly reactive (001) facets. Also, the architecture of the heterostructure with exposure (001) facets favors the separation of photogenerated electron-hole pairs and inhibit the recombination of the electron–hole pairs resulting in the increase of the number of main superoxide and hydroxyl radicals.

A useful application of green technology can be the utilization of the synthesized photocatalysts in the remediation of the environment by decomposition of organic compounds under the sunlight.

Methods

Materials. The chemicals used in this work were of analytical reagent. Titanium n-butoxide $Ti(OBu)_4$, ruthenium chloride ($RuCl_3xH_2O$), hydrochloric acid (HCl), methylene blue (MB) and NH_4OH were purchased from Sigma-Aldrich. All solutions were prepared with distilled water.

Preparation of $Ru_xTi_{1-x}O_2$ nanobelts. The 1D (one-dimension) $Ru_xTi_{1-x}O_2$ nanobelts were synthesized via a sol-gel method described by Nguyen-Phan at al. 20. A typical synthesis implies mixing at room temperature for 30 minutes, of 14 mL of titanium n-butoxide and 14 mL of hydrochloric acid (35 wt.%). Then a desirable amount of $RuCl_3xH_2O$ was added into the solution. The mixture was stirred for 12 h at 110 °C. Finally, the resulting precipitate was washed with aqueous 0.1 M NH_4OH solution (20 ml), and with distilled water. After drying at 70 °C overnight, the products were calcinated in the air at 850 °C for 3 hours. The samples were denoted as $Ru_xTi_{1-x}O_2$, where x represented the nominal doping dosage of ruthenium (x = 0.01, 0.07 and 0.16). The TiO_2 rutile sample was synthesized by a similar method without adding $RuCl_3xH_2O$ precursor and labeled as TiO_2.

Characterization. X-Ray diffraction (XRD) of the samples was analyzed at ambient temperature on a Bruker D8 Advance diffractometer using the characteristic Kα radiation of copper at a voltage of 40 kV and a current of 40 mA. XRD patterns were collected in the 2θ range between 5° and 80°.

The UV-vis diffuse reflectance spectra of rutile $Ru_xTi_{1-x}O_2$ were obtained by using a Jasco UV-Vis V-550 spectrophotometer in the wavelength range from 200 to 900 nm with an integrating sphere assembly. The sample was diluted with MgO (ratio 1:6) and then mechanically mixed. The UV-vis absorption was transformed according to the Kubelka Munk function, $F(R_\infty)$, for infinite thick samples. The sample surface elements and their oxidation states were analyzed by Thermo Scientific K-Alpha X-ray Photoelectron Spectrometer (XPS) system with Al K-alfa radiation. The Raman spectra of samples were registered using a DXR Raman Microscope from Thermo Scientific. The morphology of the samples was characterized by transmission electron microscope Tecnai™ G2 F20 TWIN

Cryo-TEM, FEI Company™, through bright field (BF-TEM) and scanning transmission electron microscopy analyses. The TEM was operated under an acceleration voltage of 200 kV. A small drop of well-dispersed sample, ultrasonicated for 5 minutes, was put on a carbon film copper grid and then, visualized on TEM.

Photocatalytic experiments. The photocatalytic studies of the rutile $Ru_xTi_{1-x}O_2$ and rutile TiO_2 composites were evaluated via the degradation of MB under sunlight with a light intensity I = 40000 lx. For photocatalysis analysis, 0,1 g of the photocatalyst was suspended in a beaker with 50 ml aqueous of MB $C_0 = 10^{-4}$ mol/l. Before exposure to sunlight, the reaction systems were kept in the dark for 30 min to reach absorption-desorption equilibrium between $Ru_xTi_{1-x}O_2$ photocatalysts and MB solution. The absorption intensity of MB was monitoring by using a UV-vis spectrophotometer Jasco UV-vis V-540. At 30 min intervals, 2 ml solution was collected and it was measured absorption at 665 nm (sample is recovered).

The degradation efficiency (DC) of MB can be calculated via the formula:

Degradation efficiency $(DC\%) = \frac{c_o - c}{c_o}$, where C_0 *and* C are concentrations of MB initial respectively measured at every 30 min. The photodegradation of MB follows pseudo-first order kinetics.

Received: 18 June 2019; Accepted: 27 November 2019;
Published online: 11 December 2019

References

1. Shen, S. *et al.* Facile Synthesis of $Zn_{0.5}Cd_{0.5}S$ Ultrahin Nanorods on Reduced Graphene Oxide for Enhanced Photocatalytic Hydrogen Evolution under Visible Light. *ChemCatChem*. https://doi.org/10.1002/cctc.201402872 (2015).
2. Sun, S. *et al*. N-Doped TiO_2 Nanobelts with Coexposed (001) and (101) Facets and Their Highly Efficient Visible- Light-Dreven Photocatalytic Hydrogen Production. *ACS Appl. Mater. Interfaces.* **8**, 18126–18131 (2016).
3. Yang, Y. *et al*. Massive Ti^{3+} Self-Doped by the injected Electrons from External Pt and the Efficient Photocatalytic Hydrogen Production under Visible Light. *Applied Catalysis B: Environmental* **218**, 751–757 (2017).
4. Yang, Y. *et al*. A Simple and Efficient Hydrogen Production-Storage Hybrid Material System (Co/TiO_2) for Synchronizing Hydrogen Photogeneration with Uptake. *J. Mater. Chem. A* **5**, 9198–9203 (2017).
5. Yang, D. *et al.* An Efficient Photocatalyst Structure: TiO_2(B) Nanofibers with a Shell of Anatase Nanocrystals. *J. Am. Chem. Soc.* **131**, 17885–17893 (2009).
6. Chaguetmi, S. *et al*. Visible-light photocatalytic performances of TiO_2 nanobelts decorated with iron oxide nanocrystals. *RSC Adv.* **6**, 114843–114851 (2016).
7. Zhou, W. *et al.* Ag_2O/TiO_2 Nanobelts Heterostructure with Enhanced Ultraviolet and Visible Photocatalytic Activity. *ACS Appl. Mater. Interfaces.* **2**, 2385–2392 (2010).
8. Zhou, W. *et al.* Control synthesis of rutile TiO_2 microspheres, nanoflower, nanotrees and nanobelts via acid-hydrothermal method and their optical properties. *Cryst. Eng.Comm.* **13**, 4557–4563 (2011).
9. Mihai, S., Cursaru, D. L., Ghita, D. & Dinescu, A. Morpho ierarhic TiO_2 with plasmonic gold decoration for highly active photocatalysis properties. *Material Letters* **162**, 222–225 (2016).
10. Shuang, S., Lv, R., Xie, Z. & Zhang, Z. Surface Plasmon Enhanced Photocatalysis of Au/Pt-decorated TiO_2 Nanopillar Arrays *Scientific Reports*, https://doi.org/10.1038/srep26670 (2016).
11. Gu, Q., Gao, Z., Yu, S. & Xue, C. Constructin Ru/TiO_2 Heteronanostructures Toward Enhanced Photocatalytic Water Splitting via a RuO_2/TiO_2 Heterojunction and Ru/TiO_2 schottky Junction. *Adv. Mater.Interfaces* **3**, 1500631–1500638 (2016).
12. Uddin, T. *et al*. Preparation of RuO_2/TiO_2 Mesoporous Heterostructures and Rationalization of Their Enhanced Photocatalytic Properties by Band Alignment Investigations. *J. Phys. Chem. C* **117**, 22098–22110 (2013).
13. Yang, H. G. *et al.* Anatase TiO_2 single crystals with a large percentage of reactive facets. *Nature* **453**, 638–641 (2008).
14. Zhao, Z., Tian, J., Sang,Y., Cabot, A. & Liu, H.Structure, Synthesis, and Applications of TiO_2 Nanobelts. *Adv. Mater.*, https://doi.org/10.1002/adma.201405589 (2015).
15. Liu, M. *et al.* Anatase TiO_2 single crystals with exposed {001} and {110} facets: facile synthesis and enhanced photocatalysis. *Chem. Commun.* **46**, 1664–1666 (2010).
16. Denton, A. & Aschcroft, N. W. Vegard's Law. *Physical Review A* **43**, 3161–3164 (1991).
17. Pei, D. N. *et al*. Defective titanium dioxide single crystals exposed by high-energy {001} facets for efficient oxygen, *Nature Communications*, https://doi.org/10.1038/ncomms9696 (2015).
18. Triggs, P. & Levy, F. Optical and Electrical Properties of Ru-Doped TiO2. *Phys. Stat. Sol. B.* **129**, 363–374 (1985).
19. Nguyen-Phan, T. *et al.* Three-Dimensional Ruthenium-Doped TiO_2 Sea Urchins for Enhanced Visible-Light-Responsive H_2 Production. *Phys. Chem. Chem. Phys.*, https://doi.org/10.1039/C6CP00472E (2016).
20. Zhumei, W., Bo, L., Zhixiang, X., Yueming, L. & Zong-Yang, S. Preparation and photocatalytic properties of RuO_2/TiO_2 composite nanotube arrays. *Ceramics International* **42**, 13664–13669 (2016).
21. Huang, Y. S. & Pollak, F. H. Raman investigation of rutile RuO_2. *Solid State Communication* **43**, 921–924 (1982).
22. Jian, T. *et al.* RuO2/TiO_2 nanobelt heterostructures with enhanced photochatalytic activity and gas-phase selective oxidation of benzyl alcohol. *Solar Energy Materials & Solar Cells* **151**, 7–13 (2016).
23. Tan, H., Ye, E. Y. & Fan, W. Y. Alumina-Template Synthesis of Fluorescent RuO_2 Nanotubes Derived from $Ru_3(CO)_{12}$ Clusters. *Adv. Mater.* **18**, 619–623 (2006).
24. Bang, S. *et al.* Dual optical functionality of local surface plasmon resonance for RuO_2 nanoparticle–ZnO nanorod hybrids grown by atomic layer deposition. *J. Mater.Chem.* **22**, 14141–14148 (2012).
25. Nguyen-Phan, T. D. *et al.* Visible Light-Driven H_2 Production over Highly Dispersed Ruthenia on Rutile TiO_2 Nanorods. *ACS Catal.* **6**, 407–417 (2016).

Author contributions

S.M. wrote the main manuscript text and prepare Figures 4, 6 and graphical abstract. D.C. and S.M. were responsible with the synthesis of $Ru_xTi_{1-x}O_2$ nanobelts. D.M. was responsible with the photocatalytic experiments and prepare Figure 5. A.M.M. performed UV-vis and XPS investigations and prepared Figure 3. R.S. was responsible with TEM investigations and she prepared Figure 2. G.B. prepared XRD investigations and prepared Figure 1.

Competing interests

The authors declare no competing interests.

Additional information

Correspondence and requests for materials should be addressed to D.L.C.

Reprints and permissions information is available at www.nature.com/reprints.

Publisher's note Springer Nature remains neutral with regard to jurisdictional claims in published maps and institutional affiliations.